Colloids and Surfaces A: Physicochemical and Engineering Aspects 623 (2021) 126719

Contents lists available at ScienceDirect

Colloids and Surfaces A: Physicochemical and Engineering Aspects

journal homepage: www.elsevier.com/locate/colsurfa

Synthesis of temperature/pH dual-responsive mesoporous silica nanoparticles by surface modification and radical polymerization for anti-cancer drug delivery

Sahar Porrang [a,b], Nader Rahemi [a,b,*,1], Soodabeh Davaran [c,d], Majid Mahdavi [e,f], Belal Hassanzadeh [g]

[a] Chemical Engineering Faculty, Sahand University of Technology, Sahand New Town, Tabriz, Iran
[b] Environmental Engineering Research Centre, Sahand University of Technology, Sahand New Town, Tabriz, Iran
[c] Department of Medical Nanotechnology, Faculty of Advanced Medical Science, Tabriz University of Medical Sciences, Tabriz, Iran
[d] Research Centre for Pharmaceutical Nanotechnology, Tabriz University of Medical Sciences, Tabriz, Iran
[e] Department of Biology, Faculty of Natural Sciences, University of Tabriz, Tabriz, Iran
[f] Department of Cell and Molecular Biology, Faculty of Biological Sciences, Kharazmi University, Tehran, Iran
[g] Faculty of Veterinary Medicine, University of Tabriz, Tabriz, Iran

HIGHLIGHTS

- Synthesis of biocompatible silica nanoparticles from rice husk as an agricultural wasteHigh.
- Biocompatibility and appropriate toxicity on the MCF-7 cell line for synthesized nano carrier.
- Higher drug delivery potential of synthesized silica with temperature and pH-responsive polymeric shell.

GRAPHICAL ABSTRACT

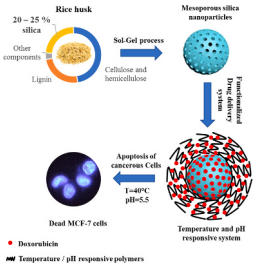

ARTICLE INFO

Keywords:
Drug delivery
Cancer treatment
Mesoporous silica nanoparticles
Rice husk
Temperature and pH-responsive
Cell apoptosis

ABSTRACT

In this study, mesoporous silica nanoparticles were synthesized from rice husk (RMSN-D) as a natural, available, economical, and non-toxic source for cancer treatment. Also, to increase the drug delivery efficiency, after modifying the surface of nanoparticles by vinyl groups (RMSN-DV), acrylic acid and n-isopropyl acrylamide were polymerized on the RMSN-DV surface by a well-tuned monomer ratio to create a biocompatible smart dual responsive drug delivery system (RMSN-DAN). The structure and physicochemical properties of the nanoparticles were characterized by XRD, FT-IR, SEM, TEM, EDS, BET, HNMR, and EDS techniques. The results indicated that monomers were successfully grafted onto the RMSN-D. Doxorubicin (Dox) was exploited as a model drug, and in-vitro Dox release was investigated. The result exhibited an excellent temperature and pH-responsive controlled release behavior. The biocompatibility and safety of natural silica source and RMSN-DAN were demonstrated Via MTT assay. Dox-loaded RMSN-DAN demonstrated cytotoxic activity similar to free Dox to MCF-7 cell line. Moreover, apoptosis of the MCF-7 cell line was investigated by flow cytometric analysis and morphological study. Therefore, this dual-responsive biocompatible and economic RMSN-DAN

* Corresponding author at: Chemical Engineering Faculty, Sahand University of Technology, Sahand New Town, Tabriz, Iran.
E-mail address: n_rahemi@sut.ac.ir (N. Rahemi).
[1] http://www.sut.ac.ir.

https://doi.org/10.1016/j.colsurfa.2021.126719
Received 16 December 2020; Received in revised form 10 April 2021; Accepted 22 April 2021
Available online 28 April 2021

nanocarrier could be applied in targeting and stimuli-responsive drug delivery due to negligible drug leakage during blood circulation whilst having a rapid release upon reaching tumor tissues.

1. Introduction

Fortunately, the use of nanocarriers to chemotherapeutic agents' delivery to the cancerous sites increases the hope of achieving a fully smart cancer-targeting system without harming normal cells. Smart drug delivery systems consist of three major components: non-toxic nanocarrier, targeting agent, and controlled drug release system. One of the main features of a nanocarrier must be its sustained release potential. Through the nanomaterials, mesoporous silica nanoparticles (MSNs), as an inorganic component have sustained drug release behavior because of structural properties [1,2]. MSNs have unique and beneficial structural properties, including high surface area, high pore volume, stable mesopore structure, adjustable pore diameter and particle size, cellular membrane-penetrating, and simple internal and external surface functionalization [3–8]. These properties have made MSNs suitable for drug delivery. The MSNs can be made of metal alkoxides such as tetraethyl orthosilicate (TEOS) [6,9–12], trimethyl orthosilicate (TMOS) [11,13,14], or inorganic metal salts such as sodium silicate [15–17]. In the previous studies, alkoxides, especially TEOS, have been commonly used as sources for the synthesis of MSNs. Due to the complicated synthesis process of the alkoxides, their high cost, and toxicity to the kidneys and respiratory tract [18], there is a tendency to synthesize MSNs from natural sources which are available, biocompatible, and non-toxic. Sodium silicate as an economical and available precursor can be an excellent source for the preparation of silica-based nanoparticles. However, industrial production of sodium silicate requires a great deal of energy. Because it is obtained by melting a mixture of high-quality sodium carbonate and quartz sand at a temperature of 1300–1600 °C [19,20], this method also produces a large volume of CO_2 gas due to burning sodium carbonate and fuel needed to reach the desired temperature [21]. Therefore, the synthesis of sodium silicate from silica-rich industrial by-products is under scrutiny. Scientists found that some agricultural wastes such as rice husk, wheat husk, etc., were a rich source of amorphous silica, which can be converted to sodium silicate [22–26]. In this case, the MSNs were obtained by hydrolysis and condensation of sodium silicate solution in the presence of surfactant under sol-gel operation [21–23]. Millions of tons of cereal husk were produced worldwide each year. Most of them were burned to generate electricity, used in construction or insulation, and the rest were disposed of as waste. The grains absorb the silica in the surrounding soil as silicic acid (water-soluble silica) through the roots and direct it to the leaves. During the evaporation and polymerization process, silicic acid was condensed to form $SiO_2.nH_2O$, and thus, the silica-cellulose hybrid membrane was formed [27]. 15–28% of rice husk dry weight is composed of silica [28,29], which is why using this material as available and economic silica sources to produce silicon-based compounds such as MSNs. Despite the remarkable features of MSNs, they were not capable of targetable drug delivery or controlled drug release. Therefore, to approach the ideal drug delivery system, the silica surface can be easily functionalized by targeting agents and controlled release systems. In this study, the functionalization of silica nanoparticles was performed to improve drug loading and targeted release. Poly (N-isopropyl acrylamide) (PNIPAAm) is a temperature-responsive polymer. Aqueous solutions of PNIPAAm become abruptly turbid at the cloud point, quickly switching to the liquid state when the temperature decreases below this point. This feature allows PNIPAAm to be used as a smart polymer in the controlled release field [30].

Moreover, Polyacrylic acid (PAA) as a pH-responsive polymer was used as the second smart polymer. The high intensity of the glycolysis process in cancerous cells results in the production of lactic acid and carbon dioxide, which causes to decrease in the pH of the cell environment. So, it can be used as an intrinsic stimulus for drug release in the target area [31]. PAA structure in the tumor extracellular environment (pH 6.8) or cancerous cell endosome and lysosome (pH 5.0–5.5) is compact. However, when the medium's pH was increased to 7.4, the carboxyl group of PAA was ionized, and the polymer expands into a fully solvated open coil format. So, this polymeric shell can act as a pH-responsive gatekeeper for controlled drug release [32]. Numerous studies have been performed to synthesize of dual stimuli-responsive copolymers such as poly (NIPAAm-co-AA) in smart drug delivery [33]. However, due to their "burst" release profile, researchers tended to use organic/inorganic composite drug delivery systems to overcome the organic drug delivery system's disadvantages and created a stable drug release profile. Thus, smart drug delivery systems were formed based on MSNs, which functionalized with smart polymers. Chang et al. synthesized magnetic MSNs coated with poly (Nisopropylacrylamide-co-methacrylic acid) (P(NIPAM-co-MAA)) to prepare dual pH and temperature-responsive system for Dox delivery. In this study, the MSN was synthesized with TEOS as a silica source. The result exhibited an apparent Thermo/pH-response controlled drug release. However, the MTT assay of blank drug delivery system to normal cells indicated that the composite microspheres were slightly toxic. At a concentration of 50 μg ml^{-1}, the cell viability was reported about 85% [34]. Zhang et al. synthesized uniform spherical regular and smooth ethane-bridged MSNs via inorganic-organic hybrid silicon sources which AA and NIPAAm monomers were grafted on vinyl modified MSNs surface [35]. Since the adjusting of monomers ratio is an essential factor in tuning the LCST and drug release efficiency, so this factor must be optimum.

Herein, we propose a facile, economic, biocompatible, safe, and efficient strategy for synthesize dual pH and thermo-responsive biogenic mesoporous silica nanoparticles, which were extracted from rice husk. High biocompatibility, good dispersity, high drug loading, higher drug release rate at the cancerous sites, and lower drug release in the normal sites due to well-tuned monomers ratio are fantastic features of the synthesized drug delivery system. This framework is providing a new approach for the study of drug loaded and controlled release behavior. Doxorubicin (Dox) has been chosen as a model chemotherapeutic agent, and HFF-2 and MCF-7 cell lines were chosen as normal and cancerous model cells, respectively. The cytotoxicity of the RMSN-D and RMSN-DAN onto the HFF-2 and MCF-7 cell lines were measured. Also, the drug release behavior of the nanocarriers in the cancerous and normal sites was investigated. Moreover, apoptosis, as the mechanism of cell death, was evaluated by a morphological study of cells and flow cytometric analysis.

2. Experimental

2.1. Materials

Rice husk as a silica bio-source, was obtained from a rice mill in Iran. Sodium hydroxide, hydrochloric acid, sulfuric acid, Cetyl trimethyl ammonium bromide (CTAB: 99%) as surfactant, sodium dodecyl sulfate (SDS) as a structure-directing agent, ammonia solution 25%, and Dimethyl sulfoxide (DMSO) were bought from Merck (Darmstadt, Germany). Triethoxyvinylsilane (TEVS: 97%) as silane coupling agent, acrylic acid (AA), n-isopropyl acrylamide 97% (NIPAAm: 97%), and potassium persulfate were purchased from Sigma-Aldrich, Chemical Co (St. Louis, MO USA). Doxorubicin hydrochloride (Dox) as a model drug was bought from the Faculty of Tabriz Pharmaceuticals, Iran. The RPMI-1640 as a cell culture medium, fetal bovine serum (FBS), and penicillin-streptomycin were procurement from Gibco (Life Technologies, Paisley, Scotland). HFF-2 and MCF-7 cell lines were obtained from the Pasteur

Institute of Iran (Tehran, Iran). The 5-diphenyl-2-H-tetrazolium bromide (MTT), Trypsin, Hoechst 33342, and Propidium Iodide powder were bought from Sigma-Aldrich, Chemical Co (St. Louis, MO USA).

2.2. Synthesis methods

2.2.1. RMSN-D synthesis

Rice husk was boiled in 1 M hydrochloric acid solution for 3 h to remove impurities. Then, the acid-treated rice husk was washed with distilled water until residual acid removal and dried overnight at 90 °C. The dried rice husk was calcinated at 550 °C for 2 h by a 5 °C/min heating rate to obtain silica nanoparticles from rice husk biosource (RSN). For the preparation of sodium silicate solution (SSS) as the RMSN-D precursor, one gram of RSN was entirely dissolved in 7.04 ml of 1 M sodium hydroxide solution. The prepared mixture was heated at 80 °C and stirred vigorously until half of the initial volume evaporated. To synthesize RMSN-D with mesoporous structure, at first, 4.8 g of CTAB as a template was added to 100 ml deionized water, and the solution was stirred at 40 °C for 1 h. Then, the SSS was dropped by drop added to the CTAB solution with the initial pH of 6.5 at 40 °C for 2 h. In the end, the pH of the mixture was adjusted to 11.25 by 1 M NaOH solution and the mixture was further stirred for 1 h. The reaction product was aged at 100 °C for 24 h. The next day, the precipitated solid product was washed with distilled water. Then it was dried at 90 °C for 12 h, and calcined at 500 °C for 4 h with a heating rate of 5 °C/min. The obtained product was assigned as RMSN-D.

2.2.2. Surface modification of RMSN-D by TEVS to RMSN-DV synthesis

The TEVS as a silane coupling agent was used to create the vinyl group on the RMSN-D. 0.1 g RMSN-D and 1.76 ml TEVS were added into the 26.6 ml ethanol and 6.6 ml deionized water, followed by ultrasonic treatment for 15 min 40 µl ammonia solution 25% was added to the solution and then was shaken for 2 h at 25 °C. Then the solution temperature was raised to 50 °C for 1 h. In the end, the modified RMSN-D was separated by centrifuging at 9000 rpm for 10 min and washed with ethanol three times. Subsequently, the resulting precipitant dried at 40 °C during the night [36].

2.2.3. Radical polymerization of AA and NIPAAm on RMSN-DV surface to RMSN-DAN synthesis

RMSN-DAN was prepared by free radical precipitation polymerization. At first, 100 mg RMSN-DV, 732 mg NIPAM, 270 µl AA, and 21.2 mg SDS were utterly dissolved in 90 ml deionized water at 70 °C for 1 h under nitrogen atmosphere. Then, the KPS solution, which was prepared by dissolving 54 mg of KPS in 5 ml deionized water, was added drop by drop in the mixture, and the reaction was accomplished at 70 °C for 6 h. The product was dialyzed (MWCO: 12,000 Da) against deionized water for three days and lyophilized to gain RMSN-DAN.

2.3. Phase transition and swelling behavior of RMSN-DAN

To evaluate the phase transition point of RMSN-DAN, 30 mg of nanoparticle was entirely dissolved in 1 ml PBS with pH equal to 5.4 at 4 °C to obtain a transparent solution of RMSN-DAN. Then the mixture temperature gradually increased. The lower critical solution temperature (LCST) was determined as the temperature when a swelling–deswelling transition suddenly occurred. Therefore, the temperature at which the solution becomes opaque was considered as the LCST point. To swelling investigation, normal and cancerous site conditions were considered. 0.3 g of RMSN-DAN was immersed in 20 ml of PBS with various solutions at the given pH and temperature for 2 days.

The swelling ratio (gram per gram) of the nanoparticle was calculated according to the following equation:

$$\text{Swelling ratio } (\%) = (W_t - W_d) * 100/W_d \quad (1)$$

W_t: swollen weight and W_d: dried weight.

2.4. Drug loading into the nanoparticles

30 mg of RMSN-D or RMSN-DAN were entirely dispersed in 3 ml deionized water at 4 °C. Then 2.25 ml of Doxorubicin solution (2 mg/ml) was added to the mixture and was stirred at 4 °C for 24 h. To obtain Dox-loaded RMSN-D and RMSN-DAN, the mixture was centrifuged at 9000 rpm for 4 min and washed with distilled water twice. The amount of loaded drug into the RMSN-D and RMSN-DAN was calculated using a UV spectrophotometer with a detection wavelength of 482 nm.

2.5. In vitro drug release behavior

To investigate the drug release behavior of nanocarriers, the Dox-loaded RMSN-D and RMSN-DAN were dispersed in 4 ml of PBS with two pH values of 7.4 and 5.4. The dispersions were transferred into a shaker incubator at the desired temperature. Then the solution was centrifuged, and the supernatant was replaced by fresh PBS at specified times. The amount of released drug was determined using a UV spectrophotometer with the detection wavelength of 482 nm.

2.6. Cell culture

Human breast cancer cells (MCF-7, cancerous cell) and Human foreskin fibroblasts cells (HFF-2, normal cell) were maintained in RPMI 1640 medium supplemented with 10% (v/v) fetal bovine serum (FBS), streptomycin (100 µg/ml), penicillin (100 U/ml) in 5% CO2 humidified atmosphere at 37 °C [32].

2.7. The cytotoxicity assays

The cytotoxicity of the RMSN-D, RMSN-DAN against HFF-2 and MCF-7 cell lines, and the Dox-loaded RMSN-D, and the Dox-loaded RMSN-DAN against MCF-7 cells were determined by MTT assay. Briefly, the HFF-2 and MCF-7 cells were seeded onto 96-well plates, in which the density of cells per well was 10^4, and incubated for 24 h to allow cell attachment. Then the cells were treated with free Dox, Dox loaded RMSN-D, and Dox loaded RMSN-DAN with the Dox concentrations ranging from 0.08 to 20 mg ml^{-1}, and blank RMSN-D, RMSN-DAN were treated with the nanocarrier's concentrations ranging from 0.4 to 200 mg ml^{-1}, respectively. After treatment, 20 µl of the MTT (5 mg/ml in PBS) was replaced in each well and incubated for an additional 3 h. Upon removing the MTT solution, the purple formazan crystals were dissolved with 100 µl DMSO, and the absorbance was recorded at 570 nm with a multi-well plate reader. Untreated cells in the medium were used as a control. All experiments were carried out with three replicates [32].

2.8. Morphological evaluation of the apoptotic cells

For morphological studies of the MCF-7 cell line, the cells were seeded in 6-well plates at a concentration of 8×10^5 cells/well, in 2 ml of the growth medium, and incubated for 24 h to allow cell attachment. After that, the cells were treated with free Dox, Dox-loaded RMSN-D, and Dox-loaded RMSN-DAN with IC 50 Doxorubicin values obtained by the MTT assay. After 48 h of incubation, The DNA was also stained with Hoechst 33258 (1 mg/ml in PBS) for 2 min, then examined using a fluorescence microscope [37].

2.9. Cell cycle analysis

To investigate the effect of drug-loaded nanoparticles on the MCF-7 cell cycle pattern, cells with a concentration of 8×10^5 were seeded in a 6-well plate. After 24 h, the cells were treated with free Dox, Dox-loaded RMSN-D, and Dox-loaded RMSN-DAN with IC 50 Doxorubicin values.

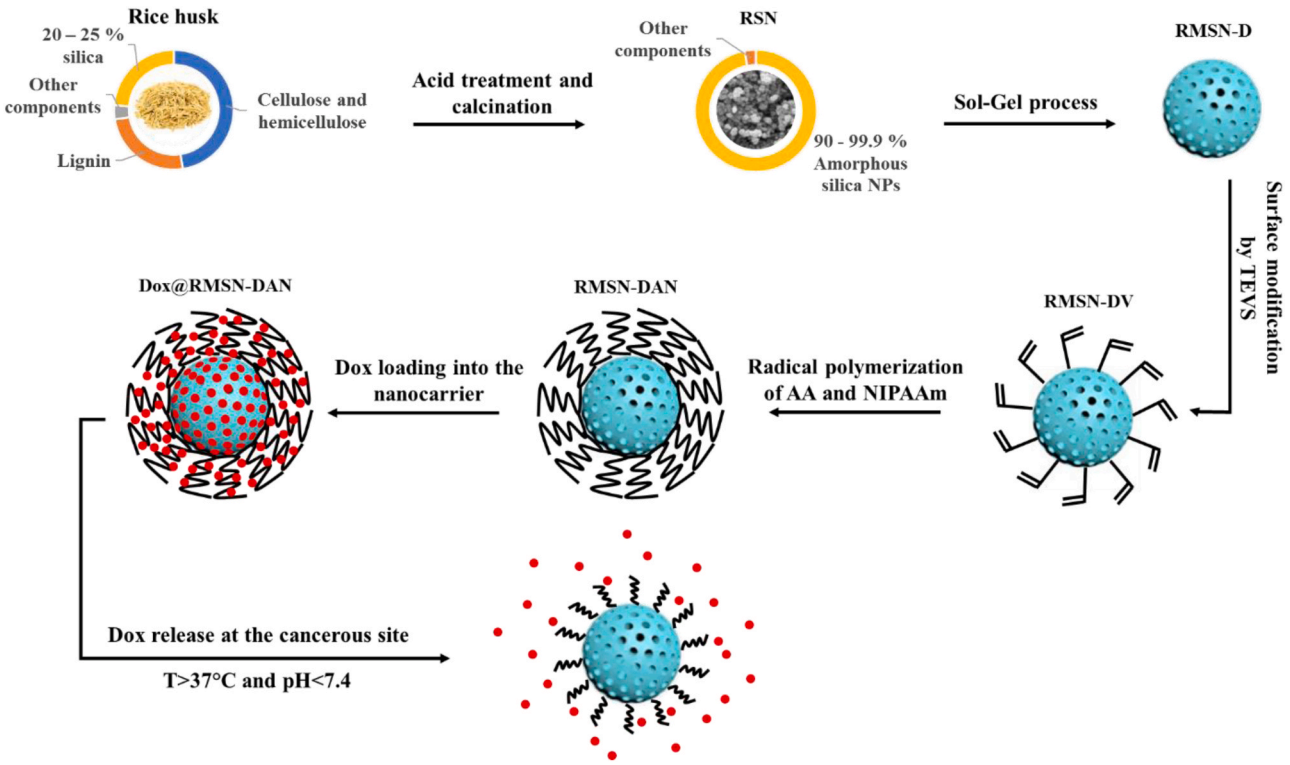

Scheme 1. The overall procedure to synthesize the RMSN-DAN nanocarriers for anti-cancer drug delivery.

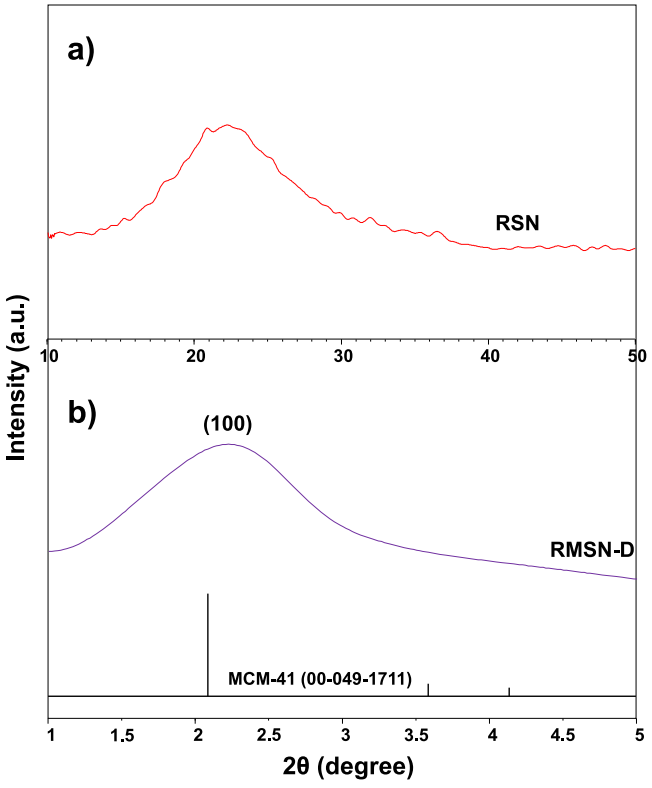

Fig. 1. X-ray diffraction patterns of the silica nanoparticles: (a) RSN and (b) RMSN-D.

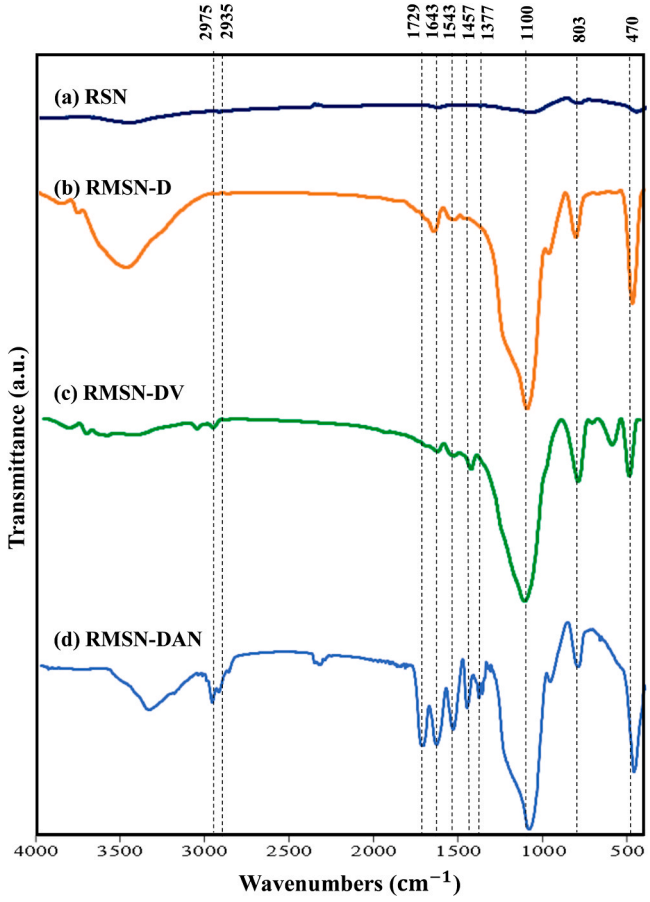

Fig. 2. FT-IR spectra of (a) RSN (b) RMSN-D (c) RMSN-D-vinyl (d) RMSN-DAN.

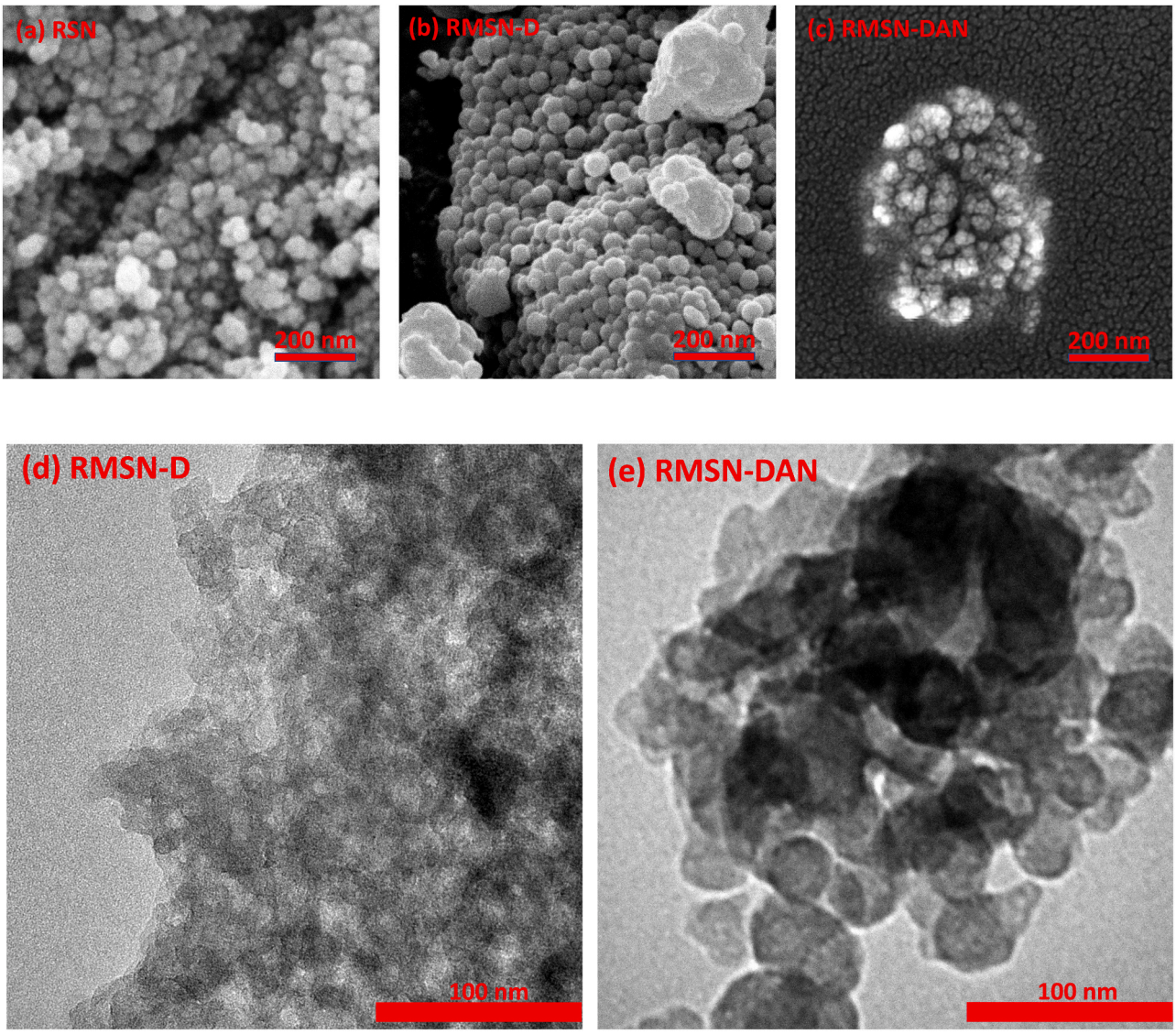

Fig. 3. SEM images of (a) RSN (b) RMSN-D (c) RMSN-DAN, and TEM images of (d) RMSN-D, and (e) RMSN-DAN.

Table 1
Mass percentage of elements in nanoparticles.

Elements (W%)	RSN	RMSN-D	RMSN-DAN
Si	63.76	71.02	10.85
O	36.24	28.98	26.61
C	–	–	50.38
N	–	–	12.16

The contents of the wells were transferred to the microtubes and washed twice by PBS. Then the cells were fixed in 600 µl ethanol (70%) and stored at 4 °C for 3 days. Then, each microtube's supernatant obtained by centrifuge, was discarded, and 100 µl Propidium iodide (PI) solution (20 µl/ml PBS) was added. In the end, the cells were analyzed by flow cytometry [38].

3. Characterization

The low angle and normal X-ray diffractometer (XRD) patterns of nanoparticles were recorded using a powder X-ray diffractometer (D8 Advance, Bruker AXS, Germany) with the scattering angle (2θ) range of 10–80° for the RSN, and 1–10° for RMSN-D. Fourier transform infrared (FT-IR) spectra were recorded using the FT-IR spectrophotometer (TENSOR 27, Bruker, Germany). The nanoparticles were visualized by scanning electron microscopy (SEM) (TESCAN Vega 3, Kohoutovice, Czech Republic) and TEM (Bruker, Germany). Moreover, the energy-dispersive X-ray spectrum (EDS) was taken. N2 adsorption-desorption isotherms and parameters such as surface area, pore size, and pore volume were obtained with Surface Area and Pore Size Distribution Analyzer (Belsorp mini, japan).

4. Results and discussion

4.1. Characterization

The overall procedure used to synthesize the RMSN-DAN is illustrated in Scheme 1.

For the synthesis of MSNs from biogenic sources, amorphous biosilica nanoparticles were first synthesized from rice husk as a precursor for the sol-gel process. Fig. 1a illustrates the RSN wide-angle XRD pattern. A characteristic broad peak at a 2θ angle of 22.17°, indicated the amorphous nature of silica. Also, no impurities were observed in the profile. Fig. 1b shows the low angle XRD pattern of RMSN-D. The XRD pattern showed the crystalline state of silica with an intense peak at a 2θ

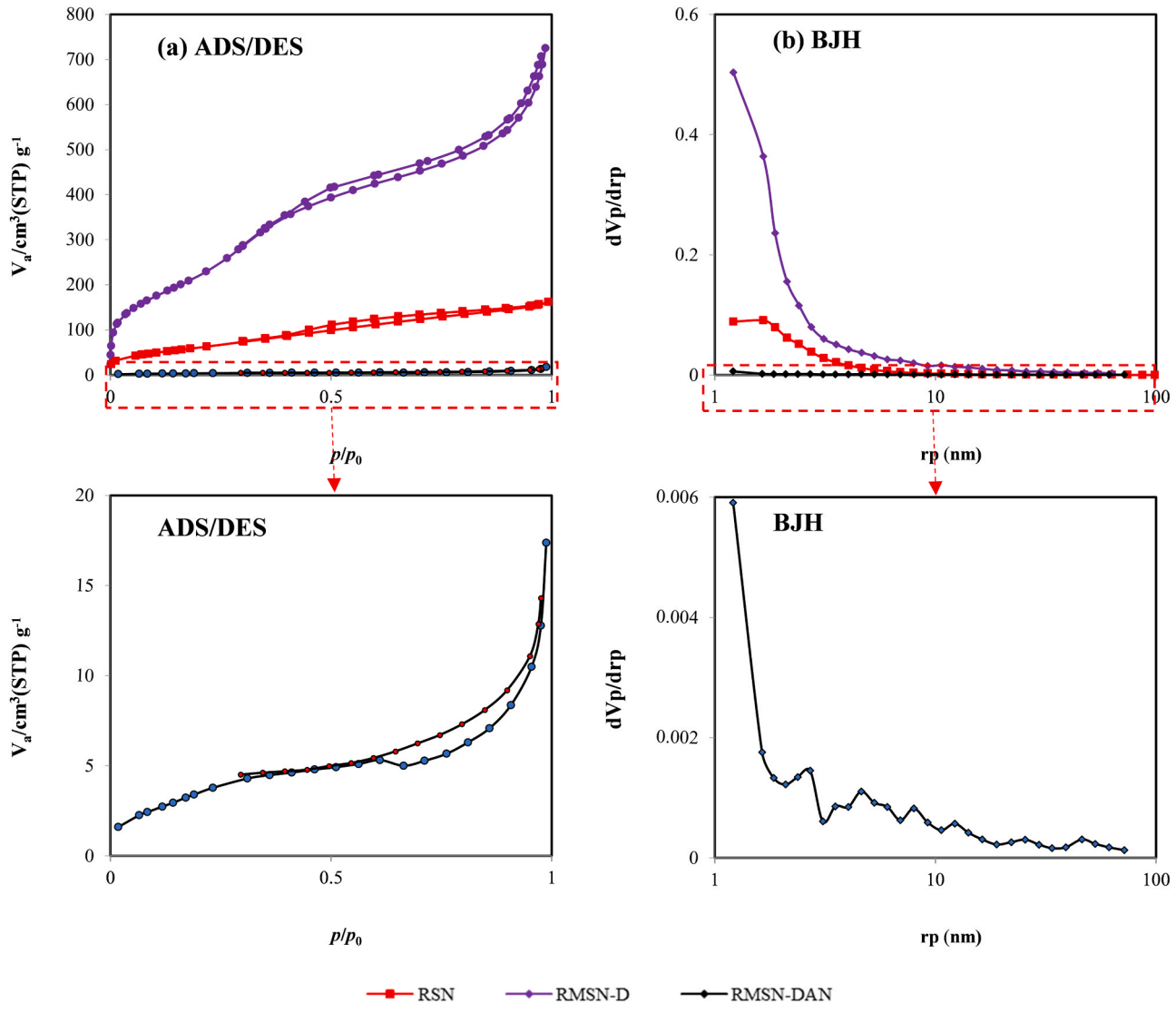

Fig. 4. The (a) N_2 adsorption-desorption isotherm and (b) BJH pore diameter distribution of RSN, RMSN-D and RMSN-DAN.

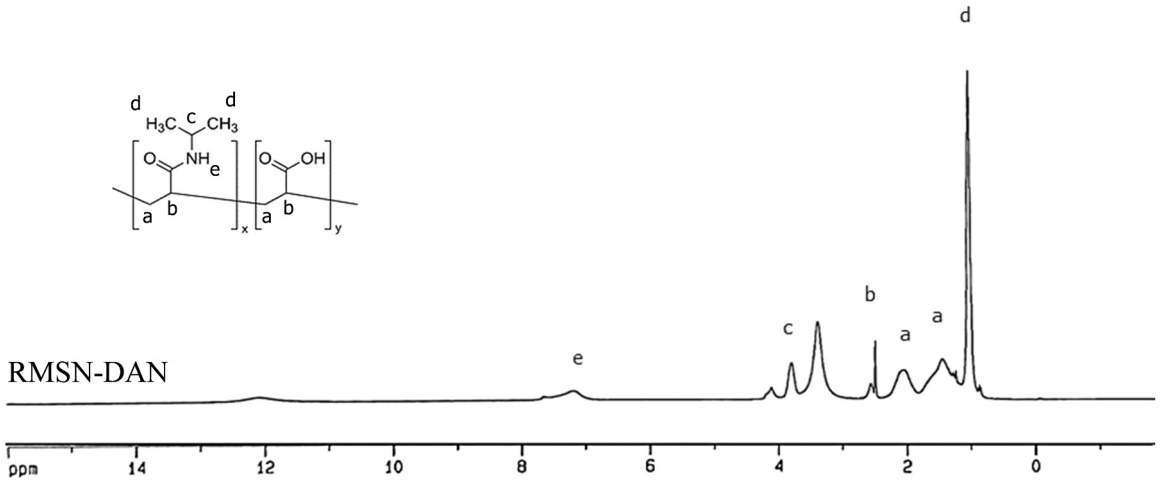

Fig. 5. ^{1}H NMR spectra of the RMSN-DAN.

= 2.36° related to the reflection line (100) for all samples, which characteristic of the hexagonal structure of the mesoporous silica nanoparticles with high crystallinity [39].

FT-IR analysis was performed to confirm the correct synthesis of RSN, RMSN-D, RMSN-DV, and RMSN-DAN nanoparticles. As illustrated in Fig. 2, characteristic bands of silica nanoparticles were visible at

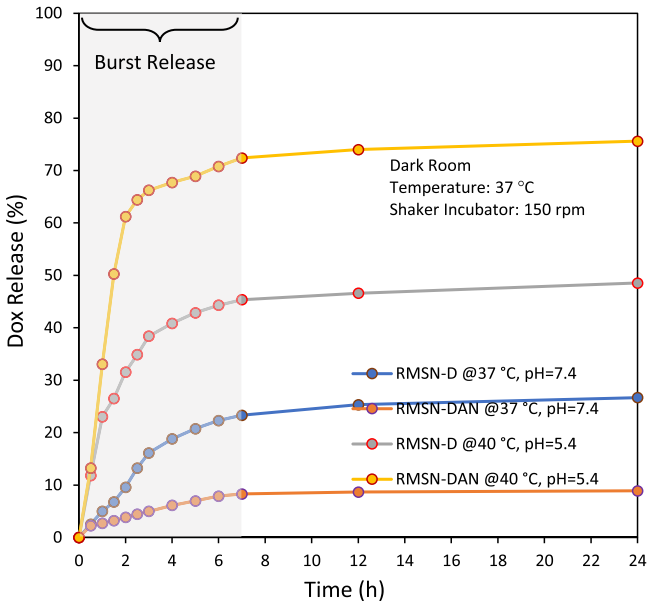

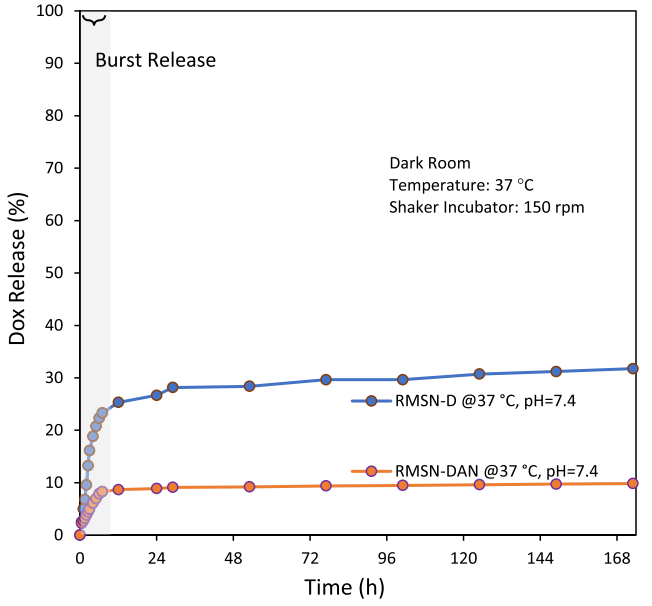

Fig. 6. Dox release profiles from Dox@RMSN-D, Dox@RMSN-DAN) (a) under cancerous, and normal cell conditions for 24 h, and (b) long time investigation under normal cell conditions.

460 cm^{-1}, 810 cm^{-1}, and 1100 cm^{-1} due to the asymmetric and symmetric stretching of Si–O–Si in all samples. The peak at 3450 cm^{-1} was related to symmetric stretching of the Si–OH group [40]. After the RMSN-D surface vinylation, the intensity of the surface silanol group decreased significantly. The C=C group of VTES was overlapped with the O–H stretching vibration of H_2O at 1620 cm^{-1}. Also, the band at 2975 cm^{-1} was associated with the C–H of vinyl groups. To ensure that the stimuli-responsive polymers were bonded to the RMSN-D surface, we need to see characteristic bands of polymers. The NIPAAm N–H stretching band was visible at 1542 cm^{-1} and C–N stretching signals at 1455 cm^{-1}, and 1385 cm^{-1} have appeared from the amide group in NIPAAm. Peaks at 1725 cm^{-1} and 1542 cm^{-1} were related to C=O, and the signal at 1639 cm^{-1} was related to C=O, and C=C groups, respectively. The peaks at 2973 cm^{-1} and 1254 cm^{-1} were owing to C–H band from the isopropyl group in NIPAAm.

The morphological properties and nanoparticles' size were analyzed by Scanning electron microscope (SEM) and Transmission electron

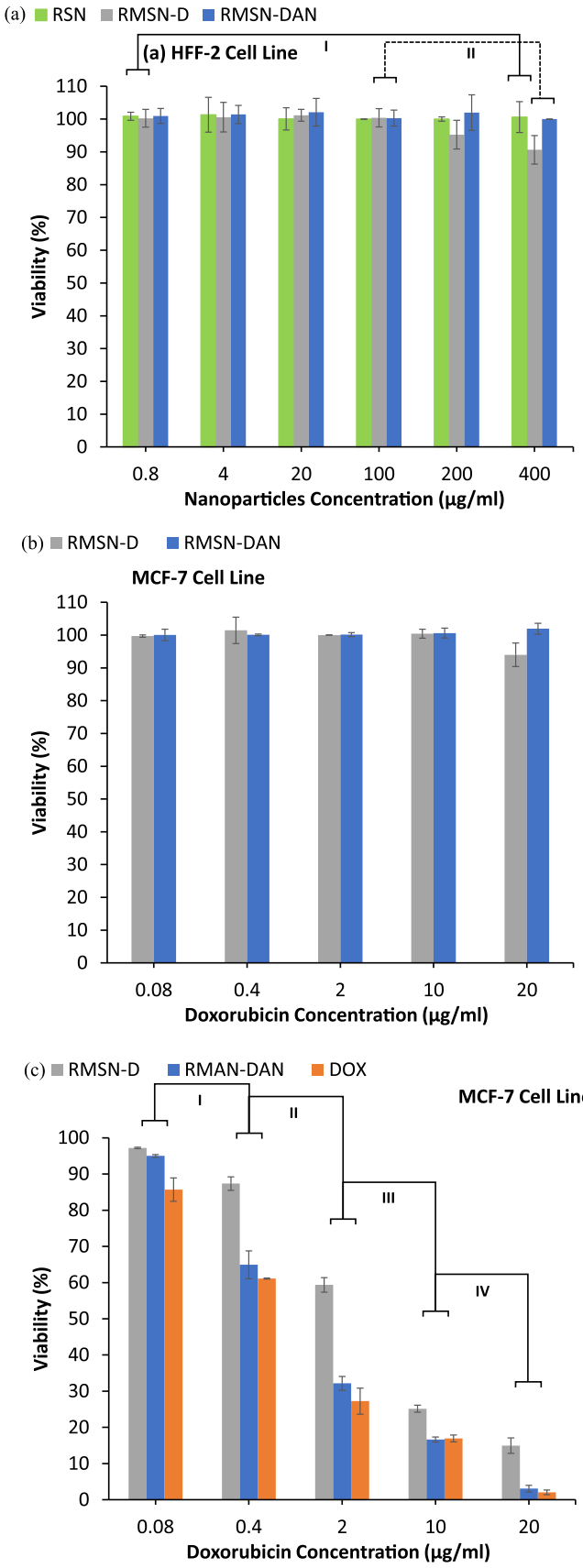

Fig. 7. The cytotoxicity and of different nanoparticles to (a) HFF-2 cells, (b) blank nanoparticles to MCF-7 cells, and (c) Dox added nanoparticles to MCF-7 cells.

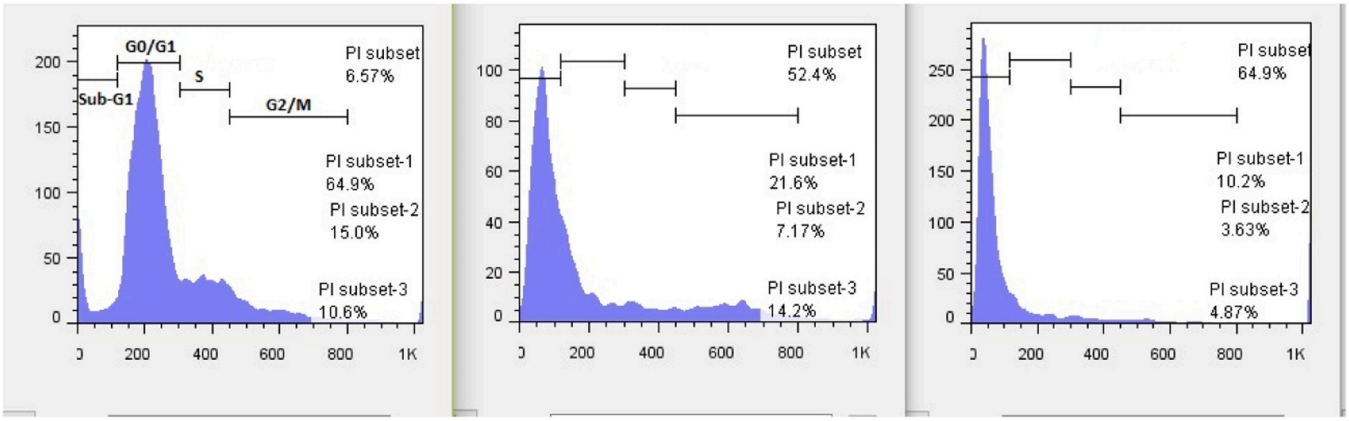

Fig. 8. Cell cycle analysis of the MCF-7 cells a) control, b) treated with Dox@RMSN-D, and c) Dox@RMSN-DAN the cells were treated with the IC50 value and harvested after 48 h.

microscope (TEM). As illustrated in Fig. 3, RSN, RMSN-D, and RMSN-DAN had a homogeneous spherical shape. The average hydrodynamic diameter of the nanoparticles was approximately 28.76, 41.8, and 34.01 nm, respectively. The size of the RMSN-DAN was smaller than RMSN-D due to the aggregation inhibitory role of polymers formed on the surface of the silica nanoparticles. The elemental analysis was determined by Energy-dispersive X-ray spectroscopy (EDS). Table 1 proposed the mass percentage of elements in nanoparticles. RSN and RMSN-D consist of Si and o elements; however, the RMSN-DAN contains Si, O, C, and N elements on its structure due to the successful conjugation of polymers on the silica surface.

To improve the drug delivery capacity, CTAB as a template was introduced to create the RMSN with a high specific surface area and appropriate total pore volume. Fig. 4a illustrated the N2 adsorption/desorption isotherms and the pore size distributions of RSN, RMSN-D, and RMSN-DAN. According to IUPAC classification, isotherms represent type IV, which confirmed the existence of a mesoporous structure. RSN and RMSN-D had a specific surface area of 226.52 and 950.76 $cm^2 g^{-1}$, respectively. Also, the average pore volume of them was 0.2498 and 1.1218 $cm^3 g^{-1}$. The corresponding pore size distribution curve (Fig. 4b) indicated that the RSN and RMSN-D had a narrow pore size. The average pore diameter of RSN and RMSN-D was 4.41 and 4.72 nm. Furthermore, the surface area, pore-volume, and pore diameter of RMSN-DAN cannot be calculated because the RMSN-D completely be trapped in the polymeric shell. So, as illustrated in Fig. 4 the N_2 adsorption-desorption parameters of RMSN-DAN cannot be detected.

The ^1H NMR spectra of the copolymers were shown in Fig. 5. The characteristic peaks attributed to the protons of NIPAAM units were observed in the ^1H NMR spectra of the RMSN-DAN. However, the peaks assigned to protons of acrylic acid were overlapped by those for the NIPAAm section. The ^1H NMR spectrum confirmed that the AA and NIPAAm were polymerized successfully on the mesoporous surface of RMSN-D.

The LCST point of RMSN-DAN was determined by detecting the phase transition of RMSN-DAN solution in the PBS with pH 5.4. By increasing the temperature to 38 °C, the solution becomes opaque from the transparent state. So, 38 °C was considered as the LCST point, which is an essential parameter in drug release behavior. The swelling percentage of RMSN-DAN was investigated at the body (37 °C and pH = 7.4) and cancerous site (40 °C and pH = 5.4) conditions. The swelling percentage for 48 h was 224% and 36%, respectively. So, the RMSN-DAN nanoparticles have a more significant swelling percentage at normal tissues in the body, which act as smart gatekeepers and protect drugs from premature release. However, in cancerous site conditions, RMSN-DAN was in collapse form, and the polymeric shell allows chemotherapeutic to release.

4.2. *In-vitro drug release behavior*

The in-vitro Dox release behavior was investigated by shaking Dox loaded RMSN-D and RMSN-DAN at 37 °C, and 40 °C in the PBS with two different pH values 7.4, and 5.4, respectively, which was illustrated in Fig. 6. The drug release rate of nanoparticles was faster at pH 5.4 than pH 7.4. In the case of RMSN-D, increasing in Dox release rate can be explicated based on Dox solubility. A lower pH causes Dox amine group protonation raising. So, the hydrophilicity of Dox enhanced [41], which afforded the fast release from the RMSN-D. However, as shown in Fig. 6, by smart polymers utilization, the drug release rates have been optimized in two different pHs. At pH 7.4, there was a strong electrostatic attraction between the negatively charged carboxyl groups and the positively charged Dox molecules. So, the Dox release from the RMSN-DAN was restricted. By reducing the pH to 5.4, the carboxylic acid group was protonated; therefore, the electrostatic interaction decreased, causing the drug to be released rapidly at an acidic pH. [41]. It is well known that the LCST of PNIPAAm is about 32 °C [42]. So, the LCST must be fine-tuned for controlled release at a cancerous site. The copolymerization of NIPAAm with other monomers such as AA can modify the LCST. It has been repeatedly reported that the LCST of the copolymer was increased by increasing the AA contents in the polymerization reactions [42–46]. Due to the higher temperature of cancerous sited than normal tissues, it is necessary to increased LCST above 37 °C with well-tuning the ratio of the monomers. In this research, the LCST was tuned at 38 °C. So, at 40 °C, which the temperature was above the RMSN-DAN LCST point, the PNIPAM was in a collapse, hydrophobic state, and consequently allowed the water-soluble Dox to diffuse out quickly from the nanoparticle shell [47, 48]. At pH 7.4, and 37 °C, which simulated the body condition, the amount of cumulative drug released from RMSN-DAN was about 8.8% in 24 h and 9.8% for 7days, which was significantly lower than that of RMSN-D (26.6% in 24 h and 31.7% during 7days). However, at pH 5.4 and 40 °C, which simulated the cancerous sites, the cumulative released drug from RMSN-DAN quickly improved to 72% in 7 h, 75% in 24 h, and was significantly higher than the cumulative released drug from RMSN-D at the same condition (45.3% in 7 h and 48.5% in 24 h). The results clearly showed the RMSN-DAN improved drug release efficiency in cancerous sites and reduced the amount of cumulative released drugs in the normal sites of the body.

4.3. *MTT assay*

To evaluate the in-vitro cytotoxicity and biocompatibility of blank nanoparticles on the normal body cells, the MTT assay was applied on the HFF-2 cell line with the nanoparticle's concentrations ranging from

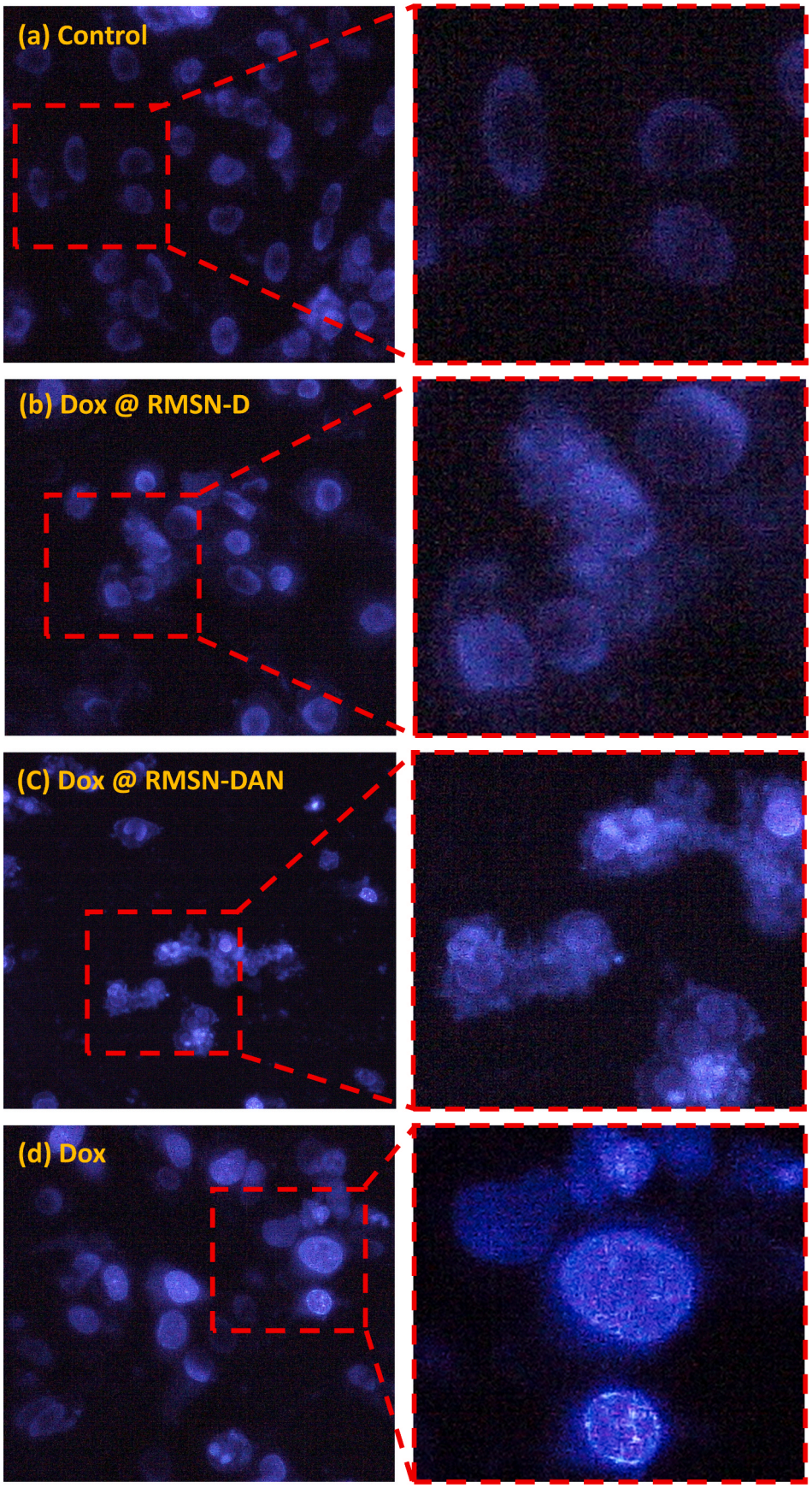

Fig. 9. Fluorescence microscopy of the MCF-7 cells treated with the a) control, b) treated with Dox@RMSN-D, c) Dox@RMSN-D-AA-NIPAAm, and d) Dox. Fluorescence images of the cells stained with Hoechst 33258 after 48 h. All the investigated chromenes induced condensation and fragmentation of the nuclei.5166737641.

0.8 to 400 μg ml^{-1}. The toxicity of RSN, RMSN-D, and RMSN-DAN was presented in Fig. 7a. Observations showed high biocompatibility and safety of RSN as a natural silica source. However, in a study compiled by A. A. Haroun et al., The viability percentage of HFB4 as a normal melanocyte cell treated by TEOS for 48 h, was less than 85% at a concentration of 100 μg ml^{-1} [49]. Also, no significant toxicity of the nanoparticles was observed due to using the non-toxic silica source and biocompatible polymers. These results showed high biocompatibility of the RMSN-D synthesis based on biosource, and RMSN-DAN, which was modified by biocompatible polymers. The potential of Dox-loaded RMSN-D and Dox-loaded RMSN-DAN as drug delivery systems for cancer therapy was investigated by evaluating Fig. 7b. In the same Dox concentrations, Dox-loaded RMSN-DAN showed higher toxicity than Dox-loaded RMSN-D due to higher releasing efficiency. It was noteworthy that the Dox-loaded RMSN-DAN toxicity effect on MCF-7 was similar to the Dox toxicity effect. So, this system can act as a high-efficiency drug delivery system in cancer therapy. Also, as expected, the blank RMSN-D and RMSN-DAN were not toxic to the MCF-7 cell line.

4.4. Cell cycle inhabitation

To determine the cell cycle distribution pattern of treated and untreated MCF-7 cells by Dox-loaded nanocarriers, a flow cytometric was performed. The cells were treated for 48 with an IC50 value of Dox-loaded RMSN-D and Dox-loaded RMSN-DAN; Then, they were analyzed by flow cytometry. As shown in Fig. 8, the control MCF-7 cells were distributed among Sub-G1, G0/G1, S, and G2/M phases by almost 6.57%, 64.9%, 15.00%, and 10.60%, respectively. After the treatment of cells with Dox-loaded RMSN-D and Dox-loaded RMSN-DAN for 48 h, the percent of the Sub-G1 phase was increased to 52.40%, and 64.9%, respectively. The results showed that the Dox-loaded nanoparticles, specially Dox-loaded RMSN-DAN, arrest the cell cycle in the Sub-G1 phase [38] and induced a high level of apoptosis in the MCF-7 cells.

4.5. Morphological assay of the apoptotic cells

The cells were cultured at a density of 8×10^5 cells/well with the indicated concentrations (IC50 Values) of the Dox-loaded RMSN-D, Dox-loaded RMSN-DAN, and Dox for 48 h. Harvested cells were stained with Hoechst 33258 to detect the apoptotic cells (Fig. 9). Under a fluorescence microscope, the control cell nucleus was large and round, without any condensation and fragmentation. However, cells treated by Dox-loaded RMSN-D, Dox-loaded RMSN-DAN, and Dox exhibited chromatin condensation and fragmentation, a typical morphological feature of apoptosis. As illustrated in Fig. 9, the chromatin condensation and fragmentation were more comprehensive in the cells were treated by Dox-loaded RMSN-DAN. These data indicate that the Dox-loaded nanocarriers caused apoptosis in the MCF-7 cell line [50].

5. Conclusion

In the present study, an economical, safe, biocompatible, and well-tuned dual-responsive drug delivery system based on a natural source was synthesized. Biogenic mesoporous silica nanoparticles were synthesis from rice husk, then AA and NIPAAm monomers were grafted on a modified RMSN-DV surface. The results demonstrate the temperature and pH-responsive polymeric shell of the RMSN-DAN can control the opening and closing of the pores. The nanocarrier's LCST was adjusted at 38 °C by monomers ratio tuning in the reaction mixture. So, the drug release can be controlled in response to environmental stimuli such as temperature and pH. Also, the cytotoxic activity and apoptosis induction of the RMSN-DAN was explored on the HFF-2 and MCF-7 cells as a model normal and cancerous cell, respectively. The biocompatibility and safety of natural silica source and RMSN-DAN were demonstrated Via MTT assay on the HFF-2 cell. Dox-loaded RMSN-DAN demonstrated cytotoxic activity similar to free Dox to MCF-7 cell line. So, RMSN-DAN had the a high potential application in temperature and pH-responsive controlled drug release and cancer treatment.

CRediT authorship contribution statement

Sahar Porrang: Conceptualization, Methodology, Visualization, Investigation, Writing - original draft. **Nader Rahemi:** Supervision, Data curation, Validation, Funding acquisition, Writing - review & editing. **Soodabeh Davaran:** Supervision, Data curation. **Majid Mahdavi:** Supervision, Data curation. **Belal Hassanzadeh:** Supervision, Data curation.

Declaration of Competing Interest

The authors declare that they have no known competing financial interests or personal relationships that could have appeared to influence the work reported in this paper.

Acknowledgments

The authors gratefully acknowledge Iran National Science Foundation (INSF), Iran for the financial support of the research under project number of 97014149 as well as Sahand University of Technology, Iran for complementary financial supports.

References

[1] Y. Wang, Q. Zhao, N. Han, L. Bai, J. Li, J. Liu, E. Che, L. Hu, Q. Zhang, T. Jiang, S. Wang, Mesoporous silica nanoparticles in drug delivery and biomedical applications, Nanomed. Nanotechnol. Biol. Med. 11 (2) (2015) 313–327.
[2] X. Yuan, S. Peng, W. Lin, J. Wang, L. Zhang, Multistage pH-responsive mesoporous silica nanohybrids with charge reversal and intracellular release for efficient anticancer drug delivery, J. Colloid Interface Sci. 555 (2019) 82–93.
[3] N. Hao, L. Li, F. Tang, Roles of particle size, shape and surface chemistry of mesoporous silica nanomaterials on biological systems, Int. Mater. Rev. 62 (2) (2017) 57–77.
[4] X. Lv, L. Zhang, F. Xing, H. Lin, Controlled synthesis of monodispersed mesoporous silica nanoparticles: particle size tuning and formation mechanism investigation, Microporous Mesoporous Mater. 225 (2016) 238–244.
[5] F. Tang, L. Li, D. Chen, Mesoporous silica nanoparticles: synthesis, biocompatibility and drug delivery, Adv. Mater. 24 (12) (2012) 1504–1534.
[6] M.E. Peralta, S.A. Jadhav, G. Magnacca, D. Scalarone, D.O. Mártire, M.E. Parolo, L. Carlos, Synthesis and in vitro testing of thermoresponsive polymer-grafted core-shell magnetic mesoporous silica nanoparticles for efficient controlled and targeted drug delivery, J. Colloid Interface Sci. 544 (2019) 198–205.
[7] Z. Mai, J. Chen, Y. Hu, F. Liu, B. Fu, H. Zhang, X. Dong, W. Huang, W. Zhou, Novel functional mesoporous silica nanoparticles loaded with vitamin E acetate as smart platforms for pH responsive delivery with high bioactivity, J. Colloid Interface Sci. 508 (2017) 184–195.
[8] X. Zhang, X. Zhang, S. Wang, M. Liu, Y. Zhang, L. Tao, Y. Wei, Facile incorporation of aggregation-induced emission materials into mesoporous silica nanoparticles for intracellular imaging and cancer therapy, ACS Appl. Mater. Interfaces 5 (6) (2013) 1943–1947.
[9] E. Ahmadi, N. Dehghannejad, S. Hashemikia, M. Ghasemnejad, H. Tabebordbar, Synthesis and surface modification of mesoporous silica nanoparticles and its application as carriers for sustained drug delivery, Drug Deliv. 21 (3) (2014) 164–172.
[10] M.C. Gomes, Â. Cunha, T. Trindade, J.P.C. Tomé, The role of surface functionalization of silica nanoparticles for bioimaging, J. Innov. Opt. Health Sci. 09 (04) (2016), 1630005.
[11] R. Narayan, U.Y. Nayak, A.M. Raichur, S. Garg, Mesoporous silica nanoparticles: a comprehensive review on synthesis and recent advances, Pharmaceutics 10 (3) (2018) 118.
[12] V. Nairi, L. Medda, M. Monduzzi, A. Salis, Adsorption and release of ampicillin antibiotic from ordered mesoporous silica, J. Colloid Interface Sci. 497 (2017) 217–225.
[13] L. Ernawati, R. Balgis, T. Ogi, K. Okuyama, Tunable synthesis of mesoporous silica particles with unique radially oriented pore structures from tetramethyl orthosilicate via oil–water emulsion process, Langmuir 33 (3) (2017) 783–790.
[14] E. Gaigneaux, et al., Scientific Bases for the Preparation of Heterogeneous Catalysts, Elsevier, 2002.
[15] C. Chapa-González, A.L. Piñón-Urbina, P.E. García-Casillas, Synthesis of controlled-size silica nanoparticles from sodium metasilicate and the effect of the addition of PEG in the size distribution, Materials 11 (4) (2018) 510.

[16] H. El-Didamony, E. El-Fadaly, A.A. Amer, I.H. Abazeed, Synthesis and characterization of low cost nanosilica from sodium silicate solution and their applications in ceramic engobes, Bol. Soc. Esp. Cerám. Vidr. 59 (1) (2020) 31–43.
[17] U. Zulfiqar, T. Subhani, S.W. Husain, Synthesis of silica nanoparticles from sodium silicate under alkaline conditions, J. Sol-Gel Sci. Technol. 77 (3) (2016) 753–758.
[18] H. Nakashima, K. Omae, T. Sakai, K. Yamazaki, H. Sakurai, Acute and subchronic inhalation toxicity of tetraethoxysilane (TEOS) in mice, Arch. Toxicol. 68 (5) (1994) 277–283.
[19] Q. Alam, Y. Hendrix, L. Thijs, A. Lazaro, K. Schollbach, H.J.H. Brouwers, Novel low temperature synthesis of sodium silicate and ordered mesoporous silica from incineration bottom ash, J. Clean. Prod. 211 (2019) 874–883.
[20] A. Lazaro, G. Quercia, H.J.H. Brouwers, J.W. Geus, Synthesis of a green nano-silica material using beneficiated waste dunites and its application in concrete, World J. Nano Sci. Eng. 03 (2013) 41–51.
[21] K.T. Tong, R. Vinai, M.N. Soutsos, Use of Vietnamese rice husk ash for the production of sodium silicate as the activator for alkali-activated binders, J. Clean. Prod. 201 (2018) 272–286.
[22] S. Chiarakorn, T. Areerob, N. Grisdanurak, Influence of functional silanes on hydrophobicity of MCM-41 synthesized from rice husk, Sci. Technol. Adv. Mater. 8 (1–2) (2007) 110–115.
[23] N. Renuka, A. Praveen, K. Anas, Influence of CTAB molar ratio in tuning the texture of rice husk silica into MCM 41 and SBA-16, Mater. Lett. 109 (2013) 70–73.
[24] M.K. Seliem, S. Komarneni, M.R.A. Khadra, Phosphate removal from solution by composite of MCM-41 silica with rice husk: kinetic and equilibrium studies, Microporous Mesoporous Mater. 224 (2016) 51–57.
[25] A. Espíndola-Gonzalez, A.L. Martínez-Hernández, C. Angeles-Chávez, V. M. Castaño, C. Velasco-Santos, Novel crystalline SiO(2) nanoparticles via annelids bioprocessing of agro-industrial wastes, Nanoscale Res. Lett. 5 (9) (2010) 1408–1417.
[26] I.R. Shaikh, A.A. Shaikh, Utilization of wheat husk ash as silica source for the synthesis of MCM-41 type mesoporous silicates: a sustainable approach towards valorization of the agricultural waste stream, Res. J. Chem. Sci. ISSN 2231 (2013) 606X.
[27] H.-P. Hentze, S.R. Raghavan, C.A. McKelvey, E.W. Kaler, Silica hollow spheres by templating of catanionic vesicles, Langmuir 19 (4) (2003) 1069–1074.
[28] M. Mandal, M. Kruk, Family of single-micelle-templated organosilica hollow nanospheres and nanotubes synthesized through adjustment of organosilica/surfactant ratio, Chem. Mater. 24 (1) (2012) 123–132.
[29] J. Tang, J. Liu, P. Wang, H. Zhong, Q. Yang, Evolution from hollow nanospheres to highly ordered FDU-12 induced by inorganic salts under weak acidic conditions, Microporous Mesoporous Mater. 127 (1–2) (2010) 119–125.
[30] S. Lanzalaco, E. Armelin, Poly (n-isopropylacrylamide) and copolymers: a review on recent progresses in biomedical applications, Gels 3 (4) (2017) 36.
[31] L. Zhang, T. Wang, L. Yang, C. Liu, C. Wang, H. Liu, Y.A. Wang, Z. Su, General route to multifunctional uniform yolk/mesoporous silica shell nanocapsules: a platform for simultaneous cancer-targeted imaging and magnetically guided drug delivery, Chem. Eur. J. 18 (39) (2012) 12512–12521.
[32] X. Hu, X. Hao, Y. Wu, J. Zhang, X. Zhang, P.C. Wang, G. Zou, X.J. Liang, Multifunctional hybrid silica nanoparticles for controlled doxorubicin loading and release with thermal and pH dual response, J. Mater. Chem. B 1 (8) (2013) 1109–1118.
[33] X.Q. Jin, et al., Dual stimuli-responsive poly (N-isopropylacrylamide-co-acrylic acid) copolymers and their applications in Ibuprofen Delivery, Int. J. Pharm. Sci. Res. 8 (6) (2017) 2421–2432.
[34] B. Chang, X. Sha, J. Guo, Y. Jiao, C. Wang, W. Yang, Thermo and pH dual responsive, polymer shell coated, magnetic mesoporous silica nanoparticles for controlled drug release, J. Mater. Chem. 21 (25) (2011) 9239–9247.
[35] K. Zhang, D. Zhou, Z. Wang, Y. Zhang, P. He, Hybrid mesoporous silica nanospheres modified by poly (NIPAM-co-AA) for drug delivery, Nanotechnology 30 (35) (2019), 355604.
[36] F. Ahangaran, A. Hassanzadeh, S. Nouri, Surface modification of Fe3O4@SiO2 microsphere by silane coupling agent, Int. Nano Lett. 3 (1) (2013) 23.
[37] H. Aryapour, M. Mahdavi, S.R. Mohebbi, M.R. Zali, A. Foroumadi, Anti-proliferative and apoptotic effects of the derivatives from 4-aryl-4H-chromene family on human leukemia K562 cells, Arch. Pharm. Res. 35 (9) (2012) 1573–1582.
[38] M. Mehdipour, G. Dehghan, R. Yekta, M. Hanifeh Ahagh, M. Mahdavi, Z. Ghasemi, Z. Fathi, DNA-binding affinity, cytotoxicity, apoptosis, cell cycle inhibition and molecular docking studies of a new stilbene derivative, Nucleosides Nucleotides Nucleic Acids 38 (2) (2019) 101–118.
[39] N. La-Salvia, J.J. Lovón-Quintana, A.S.P. Lovón, G.P. Valença, Influence of aluminum addition in the framework of MCM-41 mesoporous molecular sieve synthesized by non-hydrothermal method in an alkali-free system, Mater. Res. 20 (6) (2017) 1461–1469.
[40] Y. Yang, Y. Lin, D. Di, X. Zhang, D. Wang, Q. Zhao, S. Wang, Gold nanoparticle-gated mesoporous silica as redox-triggered drug delivery for chemo-photothermal synergistic therapy, J. Colloid Interface Sci. 508 (2017) 323–331.
[41] X. Hu, W. Wei, X. Qi, H. Yu, L. Feng, J. Li, S. Wang, J. Zhang, W. Dong, Preparation and characterization of a novel pH-sensitive salecan-g-poly (acrylic acid) hydrogel for controlled release of doxorubicin, J. Mater. Chem. B 3 (13) (2015) 2685–2697.
[42] S.J. Lue, C.-H. Chen, C.-M. Shih, Tuning of lower critical solution temperature (LCST) of poly (N-isopropylacrylamide-co-acrylic acid) hydrogels, J. Macromol. Sci. Part B 50 (3) (2011) 563–579.
[43] M.K. Yoo, Y.K. Sung, Y.M. Lee, C.S. Cho, Effect of polyelectrolyte on the lower critical solution temperature of poly (N-isopropyl acrylamide) in the poly (NIPAAm-co-acrylic acid) hydrogel, Polymer 41 (15) (2000) 5713–5719.
[44] H. Kayi, S.A. Tuncel, A. Elkamel, E. Alper, Prediction of lower critical solution temperature of N-isopropylacrylamide–acrylic acid copolymer by an artificial neural network model, J. Mol. Model. 11 (1) (2005) 55–60.
[45] S. Li, X. Liu, Synthesis, characterization, and evaluation of enzymatically degradable poly (N-isopropylacrylamide-co-acrylic acid) hydrogels for colon-specific drug delivery, Polym. Adv. Technol. 19 (11) (2008) 1536–1542.
[46] S. Liu, X. Liu, F. Li, Y. Fang, Y. Wang, J. Yu, Phase behavior of temperature-and pH-sensitive poly (acrylic acid-g-N-isopropylacrylamide) in dilute aqueous solution, J. Appl. Polym. Sci. 109 (6) (2008) 4036–4042.
[47] S.R. Deka, A. Quarta, R. Di Corato, A. Riedinger, R. Cingolani, T. Pellegrino, Magnetic nanobeads decorated by thermo-responsive PNIPAM shell as medical platforms for the efficient delivery of doxorubicin to tumour cells, Nanoscale 3 (2) (2011) 619–629.
[48] Y. Zhu, S. Kaskel, T. Ikoma, N. Hanagata, Magnetic SBA-15/poly (N-isopropylacrylamide) composite: preparation, characterization and temperature-responsive drug release property, Microporous Mesoporous Mater. 123 (1–3) (2009) 107–112.
[49] A.A. Haroun, A.M. Elnahrawy, H.I. Abd-Alla, Sol-gel preparation and in vitro cytotoxic activity of nanohybrid structures based on multi-walled carbon nanotubes and silicate, Inorg. Nano-Met. Chem. 47 (7) (2017) 1023–1027.
[50] M.H. Naseri, M. Mahdavi, J. Davoodi, S.H. Tackallou, M. Goudarzvand, S. H. Neishabouri, Up regulation of Bax and down regulation of Bcl2 during 3-NC mediated apoptosis in human cancer cells, Cancer Cell Int. 15 (1) (2015) 55.